Orographic precipitation in valley network headwaters: Constraints on the ancient Martian atmosphere

Kathleen E. Scanlon,[1] James W. Head,[1] Jean-Baptiste Madeleine,[1]
Robin D. Wordsworth,[2] and François Forget[3]

Received 9 May 2013; revised 18 June 2013; accepted 19 June 2013; published 27 August 2013.

[1] We examine the Martian valley networks in the framework of topographic influences on precipitation. We use an analytical model and the Laboratoire de Météorologie Dynamique (LMD) early Mars global circulation model (GCM) to explore the local-scale distribution of orographically forced precipitation as a function of atmospheric pressure. In simulations with 500 mbar and 1 bar CO_2 atmospheres, orographic lifting results in enhanced snowfall upslope of the observed valley network tributaries. Our framework also suggests that a 2 bar atmosphere cannot create the observed valley pattern at the highest-relief valley network, Warrego Valles. As in previous work, the GCM does not generate temperatures warm enough for rain or significant snowmelt in the highlands with CO_2 greenhouse warming alone. Thus while transient periods of unusual warming are still required to melt the deposits and carve the valleys, our model predicts snow deposition in the correct locations. **Citation:** Scanlon, K. E., J. W. Head, J.-B. Madeleine, R. D. Wordsworth, and F. Forget (2013), Orographic precipitation in valley network headwaters: Constraints on the ancient Martian atmosphere, *Geophys. Res. Lett.*, *40*, 4182–4187, doi:10.1002/grl.50687.

1. Introduction

[2] Because liquid water is unstable to freezing and sublimation under current Martian surface conditions, the valley networks incising some of the oldest landscapes on Mars are often cited as evidence that the Martian climate was once warm and wet. Whether they require that ancient Mars experienced high surface pressure or temperatures warm enough for rainfall has been debated, however [e.g., *Wallace and Sagan*, 1979; *Carr*, 1983; *Squyres and Kasting*, 1994; *Craddock and Howard*, 2002; *Gaidos and Marion*, 2003]. The geomorphology of the networks can provide some insight into the climate that created them [e.g., *Craddock and Howard*, 2002; *Barnhart et al*., 2009; *Som et al*., 2009; *Irwin et al*., 2011], but the influence of ancient Martian precipitation patterns on their distribution has not been investigated in detail.

[3] When moist air is lifted, it expands and cools, allowing saturation to occur and water to condense. Topography can generate precipitation [*Giambelluca et al*., 1986] or enhance background precipitation by channeling air along convergent paths, by controlling the distribution of solar heating, or by directly forcing air to rise as the ground rises beneath it [*Roe*, 2005; *Smith*, 2006; *Houze*, 2012]. If the valley networks were formed by precipitation, at a minimum their distribution should reflect enhanced water supply where orographic lifting of moist air is predicted.

[4] Orographic precipitation has been suggested to be an important influence on the distribution of water ice on recent Mars [*Forget et al*., 2006]. It should have been even more important for early Mars if the late Noachian–early Hesperian atmospheric pressure was at least a few hundred millibars: more water can precipitate from a warmer atmosphere, and the altitude dependence of the surface temperature (surface lapse rate) is greater in a thicker atmosphere due to increased thermal coupling between the atmosphere and surface, such that snow and ice deposits are more stable at high altitudes [*Forget et al*., 2013; *Wordsworth et al*., 2013].

[5] Topographic effects on insolation can exert a strong control on recent Martian fluvial activity by controlling the location of snow and ice stability and melt [e.g., *Costard et al*., 2002; *Balme et al*., 2006; *Dickson et al*., 2007; *Williams et al*., 2009; *Morgan et al*., 2010], but they are unlikely to have been an important factor in the distribution of the valley networks. Most of the valleys lie within 30° of the equator, where insolation is only weakly slope-dependent even today [*Kreslavsky et al*., 2008]. If the valleys were carved in an atmosphere with at least a few hundred millibars of CO_2, stronger radiative and sensible heat coupling between the surface and atmosphere (notably because of scattering by CO_2 and water ice clouds) could further homogenize surface insolation and the energy balance.

[6] Since it is not currently feasible to run general circulation models (GCMs) at a grid spacing that can resolve topography at the scales on which the density of the valley networks varies, a downscaling approach is necessary to investigate the influence of individual Martian ridges on precipitation patterns and amount. The orographic precipitation model of *Smith and Barstad* [2004] uses large-scale climate fields and topographic data to calculate precipitation forced directly by orographic lifting, producing precipitation maps at the resolution of the topographic data. We used Mars

[1]Department of Geological Sciences, Brown University, Providence, Rhode Island, USA.
[2]Department of Geophysical Sciences, University of Chicago, Chicago, Illinois, USA.
[3]Laboratoire de Météorologie Dynamique, Institut Pierre Simon Laplace, Paris, France.

Corresponding author: K. E. Scanlon, Department of Geological Sciences, Brown University, 324 Brook St., Providence, RI 02912, USA. (kathleen_scanlon@brown.edu)

0094-8276/13/10.1002/grl.50687

Orbital Laser Altimeter (MOLA) topography data and climate fields from the Laboratoire de Météorologie Dynamique (LMD) generic model adapted to early Mars [*Wordsworth et al*., 2011; *Forget et al*., 2013; *Wordsworth et al*., 2013] as input to this model.

2. Methods

[7] We chose regions of study to satisfy three criteria. First, valleys in the region should be late Noachian-early Hesperian in age [*Irwin and Howard*, 2002; *Fassett and Head*, 2008; *Hoke and Hynek*, 2009]. Second, valley networks should appear relatively well preserved, unaltered by subsequent impacts, superposed lava flows, and erosion, ensuring that the current valley distribution reflects the distribution of emplacement as closely as possible. Finally, well-preserved valleys should be present on regional slopes facing in more than one direction so that valleys on different aspects can be compared. We found regions satisfying these criteria (Figure S1 in the supporting information) in Terra Cimmeria, Margaritifer Sinus (Paraná Valles and others), Terra Sabea (Tisia Valles and others), and Thaumasia Planum (Warrego Valles). We compared predicted orographic precipitation with maps of valley networks in these regions [*Hynek et al*., 2010] to which we added valleys newly visible in Mars Reconnaissance Orbiter Context Camera (CTX) and 100 m/pixel Mars Odyssey Thermal Emission Imaging System (THEMIS) daytime IR images.

[8] In all of our GCM simulations, as in prior work [*Forget et al*., 2013; *Wordsworth et al*., 2013], the surface temperature is too cold to allow sustained liquid water. If these simulations represent the typical state of early Mars, the distribution of the valley networks is a function of two climates [*Halevy and Head*, 2012; *Wordsworth et al*., 2013]: a cold "background" climate, warmed only by H_2O and CO_2 gas and clouds as in the GCM simulations, during which snow deposits would have been emplaced; and an intermittent warm climate, warmed by one or more additional greenhouse gases, during which they would have melted. In this paper, we investigate this cold end-member scenario. Therefore, the model was run until ice reached an equilibrium distribution in the highlands, where it would have melted upon the arrival of a transient warm era [*Halevy and Head*, 2012; *Wordsworth et al*., 2013].

[9] The LMD generic climate model [*Wordsworth et al*., 2011] was run in early Mars mode with a pure CO_2 atmosphere at surface pressures of 0.5 bar, 1 bar, and 2 bar, at 25° obliquity. Present-day GCM-scale topography was used. The grid spacing was 5.625° in latitude and 11.25° in longitude. All other run parameters were set as described in *Wordsworth et al*. [2013].

[10] The gridded MOLA topography used with the analytical model has 128 pixels per degree resolution. We leveled superposed fresh craters in the MOLA topography using the Photoshop CS5 heal tool [*Matsubara et al*., 2011] but otherwise left the topography unaltered from its present state.

[11] The analytical orographic precipitation model used in this study has been validated in numerous regions of the Earth [e.g., *Barstad and Smith*, 2005; *Smith et al*., 2005; *Crochet et al*., 2007; *Minder et al*., 2008; *Hughes et al*., 2009]. It is based on general equations of fluid dynamics and thermodynamics [*Smith and Barstad*, 2004] and is therefore applicable to a broad range of planetary climates. In addition to topography and wind, the model requires as input an environmental atmospheric lapse rate, a saturated adiabatic lapse rate, and a surface reference temperature. From these variables, a condensation coefficient C_w, vertical wavenumber m of topographically forced waves, moist layer depth H_w, and falling timescale τ_f can be calculated. Condensation timescales τ_c were calculated as in the GCM [*Montmessin et al*., 2002] but assuming saturation in order to remain consistent with the orographic precipitation model. Falling timescales were calculated assuming that hydrometeors are similar in shape to terrestrial snowflakes and fall at terminal velocity. The environmental lapse rate was averaged over the region of study and over a Martian year. The saturated adiabatic lapse rate was calculated for condensing water in a pure CO_2 atmosphere using the annual average surface pressure and temperature in the region of study. Wind speeds and reference temperatures used in the precipitation model were taken from ~145 m above the surface.

[12] The central model equation, which relates Fourier transformed topography $\hat{h}$ to Fourier transformed orographic precipitation $\hat{P}$, is

$$\hat{P}(k,l) = \frac{C_w i\sigma\hat{h}(k,l)}{(1 - imH_w)(1 + i\sigma\tau_c)(1 + i\sigma\tau_f)},$$

where $\sigma = Uk + Vl$. After performing an inverse Fourier transform of $\hat{P}$, negative values of precipitation are set to zero. For a detailed explanation of the model, see *Smith and Barstad* [2004].

[13] As a consequence of its mathematical formulation, the model delivers a "snapshot" of precipitation assuming constant atmospheric properties across its domain, rather than calculating a time-evolving condensation field where precipitated water is removed from the atmosphere, as a GCM would. As such, precipitation amounts are likely to be excessive downwind of topographic highs.

[14] To satisfy the validity criteria of the orographic precipitation model [*Smith*, 2006], the nondimensional parameter $UN_m^{-1}h^{-1}$ must be greater than 1, where U is the wind speed and h is the height of the obstacle. N_m is the moist buoyancy frequency given by

$$N_m = \sqrt{\frac{g(\Gamma_e - \Gamma_m)}{1000T}},$$

where g is the gravitational acceleration at the Martian surface in m/s^2, Γ_e is the environmental lapse rate in the region of study in K/km, Γ_m is the moist adiabatic lapse rate in K/km, and T is the temperature at the reference level where climate variables are calculated [*Smith*, 2006]. In other words, surface winds should have sufficient kinetic energy to flow over regional topographic obstacles rather than around them.

3. Results

3.1. Orographic Precipitation

[15] Analytical model results are consistent with a strong role for orographic precipitation. The assumption of saturation means that the modeled orographic precipitation is an overestimate and should not be considered quantitatively. As a more qualitative comparison, in our regions of study, it is largely of order 10^{-3} to 10^{-2} mm/h at 1 bar compared to average synoptic-scale precipitation of order 10^{-4} to 10^{-3} mm/h.

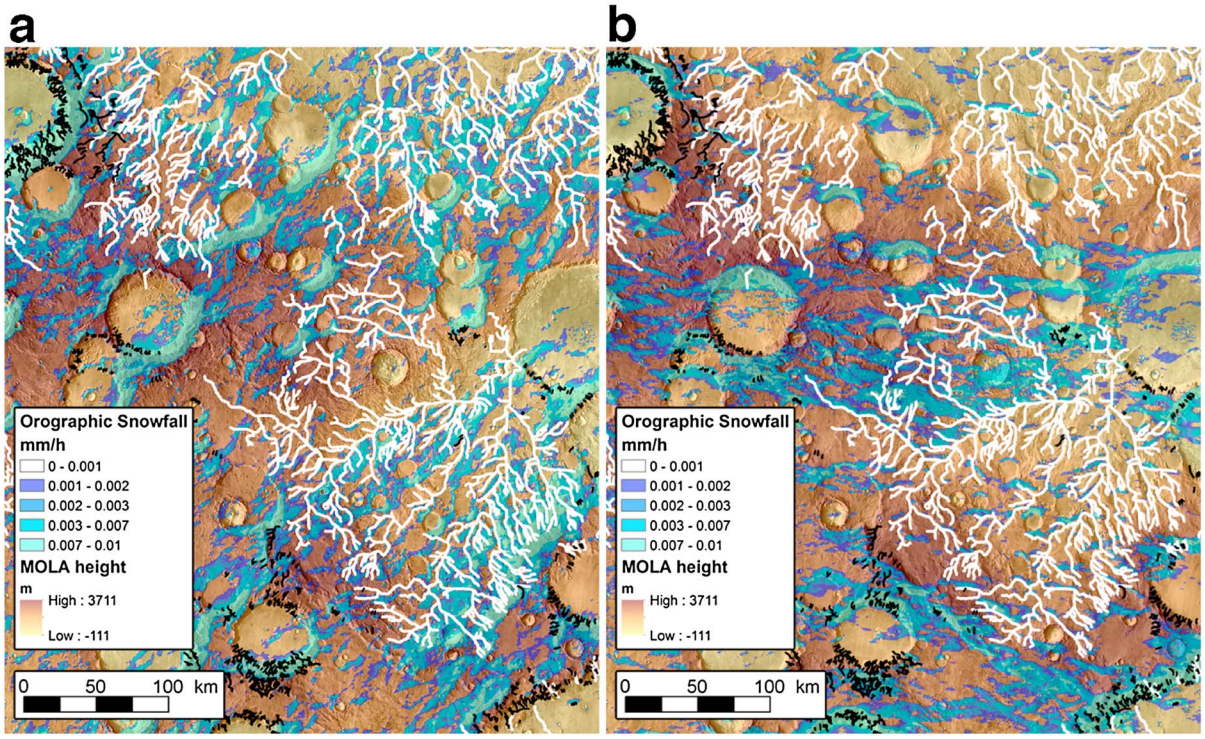

Figure 1. (a) Valley networks in Terra Cimmeria and MOLA-shaded THEMIS daytime IR imagery. The image is centered near 10.2°S, 126.2°E. Valleys mapped by *Hynek et al*. [2010] using 230 m/pixel resolution THEMIS-IR imagery are shown in white. Valleys newly visible in ~6 m/pixel resolution CTX and 100 m/pixel resolution THEMIS-IR imagery are shown in black. The rate (in mm/h) of modeled orographic precipitation forced by northwesterly winds in a 1 bar atmosphere is shown in blue. (b) As in Figure 1a but with a 4 m/s wind from the south instead of from the northwest. Very few valleys head inside regions of precipitation.

[16] Our first study area, in Terra Cimmeria, centers on a broad ridge that extends ~650 km northwest from Herschel Crater (Figure 1). Two large, dendritic valley networks dissect most of its northeast slope; smaller dendritic networks cover part of its southwestern slope. A northwesterly wind causes maxima of orographic precipitation to occur where most of the observed valleys head (Figure 1a), and in all of our GCM simulations, such winds are dominant at the nearest grid point to this location (Figure 2). For comparison, if the model is run with a wind direction that is uncommon in the GCM, very few of the valleys head near predicted precipitation maxima (Figure 1b).

[17] We also applied the models to the valleys of Margaritifer Sinus and Terra Meridiani (Figure S2). Valleys in the region preferentially form on north or west facing slopes, and westerly winds are predominant in the region in all of our GCM simulations, followed by northwesterly in all but the 2 bar case (Figure S3). The maxima of drainage density, including Paraná Valles and the valleys on Newcomb Crater, all lie on maxima of predicted orographic precipitation in a westerly wind. Several lows are much more heavily dissected on one side, and the precipitation model generally reproduces this pattern as well (for example, in the boxed region in Figure S2).

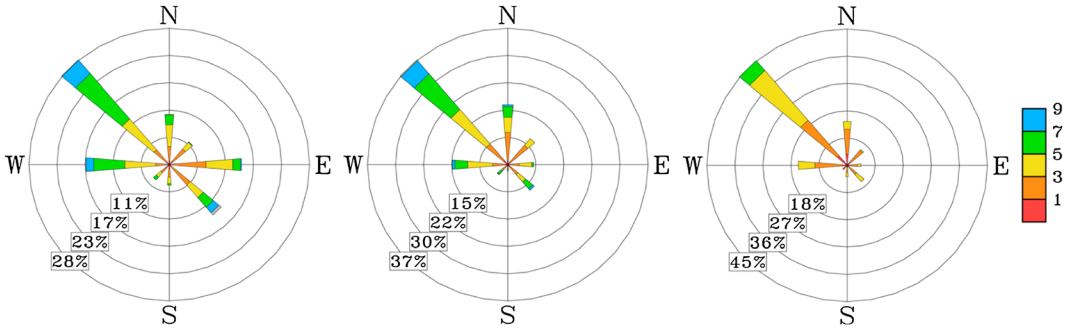

Figure 2. Wind rose diagrams for the grid box nearest the center of Figure 1a, compiled from one Mars year of our GCM simulation with (left) 500 mb, (center) 1 bar, and (right) 2 bar surface pressure. The length of each column corresponds to the frequency of winds blowing from within a 45° bin centered on each compass direction. The length of colored bands within each column indicates the frequency of the corresponding wind speed range.

Table 1. Topographic and Flow Parameters[a]

Region and P_{CO2}	Maximum Ridge Height	Wind Direction, Median Speed	Mean N_m	Median $UN_m^{-1}h^{-1}$
Terra Cimmeria, 0.5 bar	1400 m	NW, 5.3 m/s	0.003 s^{-1}	1.25
Terra Cimmeria, 1 bar		NW, 4.9 m/s	0.002 s^{-1}	1.74
Terra Cimmeria, 2 bar		NW, 3.3 m/s	0.001 s^{-1}	2.37
Margaritifer Sinus, 0.5 bar	1500 m	W, 7.0 m/s	0.003 s^{-1}	1.55
Margaritifer Sinus, 1 bar		W, 6.1 m/s	0.002 s^{-1}	2.04
Margaritifer Sinus, 2 bar		W, 4.9 m/s	0.001 s^{-1}	3.24
Terra Sabea, 0.5 bar	1400 m	NE, 4.1 m/s	0.002 s^{-1}	1.47
Terra Sabea, 1 bar		NE, 3.1 m/s	0.002 s^{-1}	1.11
Terra Sabea, 2 bar		NE, 1.6 m/s	0.001 s^{-1}	1.12
Thaumasia Plateau, 0.5 bar	2500 m	W, 6.9 m/s	0.004 s^{-1}	0.69
Thaumasia Plateau, 0.5 bar		E, 3.3 m/s	0.004 s^{-1}	0.33
Thaumasia Plateau, 1 bar		W, 6.9 m/s	0.003 s^{-1}	0.92
Thaumasia Plateau, 1 bar		E, 3.0 m/s	0.003 s^{-1}	0.40
Thaumasia Plateau, 2 bar		W, 2.5 m/s	0.002 s^{-1}	0.50
Thaumasia Plateau, 2 bar		E, 1.9 m/s	0.002 s^{-1}	0.38

[a] N_m is rounded to the nearest 0.001 s^{-1}, wind speed to the nearest 0.1 m/s, and ridge height to the nearest 100 m. Ridge height is measured from the head of the lowest tributary on a slope to its tallest point; it does not correspond with absolute elevation, but the elevation change forced on a rising air parcel.

[18] In our region of study in Terra Sabea (Figure S4), valleys preferentially form on northward and eastward facing slopes, and the orographic precipitation distribution fits observed valleys well when calculated with a northeasterly wind. Winds in this region have a northerly or easterly component for more than 90% of the year in all of our simulations (Figure S5).

3.2. Dynamical Constraints on the Noachian Climate

[19] The valley networks typically head at or near topographic divides or peaks [e.g., *Hynek and Phillips*, 2003; *Hynek et al*., 2010; *Mest et al*., 2010; *Irwin et al*., 2011], but drainage density in our regions of study does not show any clear altitude dependence. In the regions discussed above, small, dendritic or subparallel valleys incise the interior rims and walls of older craters. Since these are often densest near the maxima of the larger valleys on crater exteriors, and in many cases appear embayed by Hesperian volcanic crater fill, we interpret them as coeval with the larger valleys. If the valley networks were emplaced in a climate with slow average near-surface winds, orographic precipitation would reach a maximum partway up the slope because the humid low-level air would lack sufficient kinetic energy to ascend the entire slope. Unless synoptic or large-scale convective precipitation was so strong that it overwhelmed the signature of orographic precipitation, windward slopes would be most heavily incised well below their summits in a $U < N_m h$ regime, and leeward slopes would experience very little erosion.

[20] The relief of the incised topography at our first three sites is not great enough to allow us to constrain the early Mars CO_2 surface pressure. Median winds are fast enough at all three sites and all three surface pressures to surmount the tallest crater rims (Table 1). However, the Warrego Valles network is incised into a ~5 km rise on the Thaumasia Plateau, making it the only Noachian–Hesperian valley network suitable to test for flow regime differences between climates. Researchers using more recent imagery [*Ansan and Mangold*, 2006; *Hynek et al*., 2010] have noted that its west facing slopes are more heavily dissected than its south and east facing slopes and that the south and east facing valleys are overwhelmingly restricted to lower altitudes.

[21] Our GCM results (Figure 3) provide a robust explanation for this pattern. In our 500 mb and 1 bar simulations, the wind at the nearest grid point is predominantly from the west and would have strongly enhanced precipitation on that side of the mountain. About 41% of westerly winds are strong enough to surmount the plateau in the 1 bar climate. Southerly and easterly winds are less common and have median speeds near 3 m/s in both the 500 mb and 1 bar simulations. Rather than flowing over it, the slower southerly and easterly winds would almost always have been forced to flow around the mountain after ascending partway, resulting in

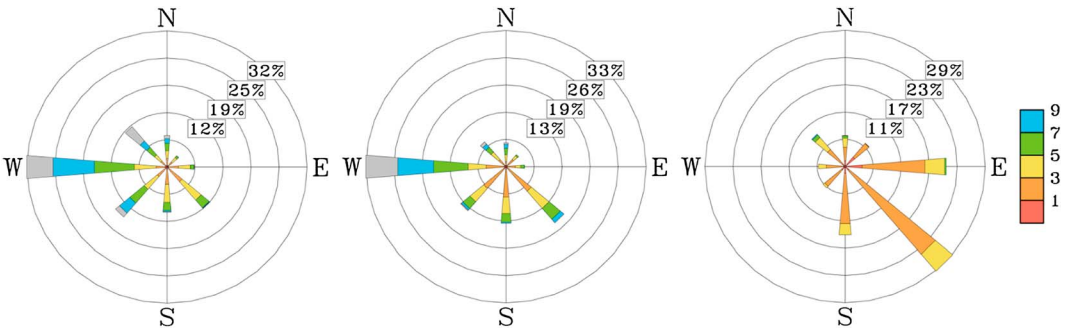

Figure 3. Wind rose diagrams for the grid box nearest the center of Warrego Valles, compiled from one Mars year of our GCM simulation with (left) 500 mb, (center) 1 bar, and (right) 2 bar surface pressure. The length of each column corresponds to the frequency of winds blowing from within a 45° bin centered on each compass direction. The length of colored bands within each column indicates the frequency of the corresponding wind speed range.

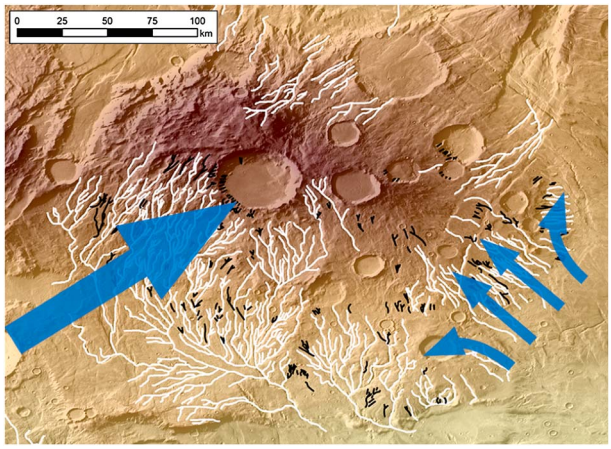

Figure 4. Schematic of flow regimes on the west facing and east facing slopes of the plateau incised by Warrego Valles. More frequent flow from the west allows more precipitation, and consequently tributary development, on west facing slopes. Stronger flow on the west allows precipitation at higher altitudes on west facing slopes than on south facing and east facing slopes.

nearly all precipitation being emplaced on the lower half of the slopes (Figure 4). The meridional temperature gradient, the wind speed, and the extent of the Hadley cell decrease with increasing surface pressure in our simulations, as in *Kerber et al*. [2013], due to the higher heat transport capacity of thicker atmospheres. In the 2 bar simulations, even the yearly maximum wind is not strong enough to produce the highest tributaries on either side, and westerly winds are rare at Warrego Valles (Figure 3) because the winter hemisphere jet no longer reaches 40°S [*Kerber et al*., 2013]. Since the 2 bar wind strength and direction are both inconsistent with observations, the distribution of Warrego Valles casts doubt on the possibility of an early Mars surface pressure of 2 bars or greater. Since no other late Noachian-early Hesperian valley networks span as broad a range of altitudes, Warrego Valles is the only region where the $U > N_m h$ criterion can be used to distinguish between climates. Crater dating indicates that the network formed contemporaneously with the majority of valley networks [*Ansan and Mangold*, 2006; *Fassett and Head*, 2008], however, suggesting that this sole available example can inform us of the general conditions at the time.

4. Discussion

[22] Recent climate modeling studies [*Wordsworth et al*., 2013] have indicated that on large scales, water in a thicker early Martian atmosphere migrates to the highlands because adiabatic cooling creates a cold trap at high altitudes. Here we have shown that additional precipitation forced by topography at scales below GCM resolution enhances this effect. Where late Noachian–early Hesperian valley networks are well preserved, we have shown that their observed maxima can be predicted by an orographic precipitation model driven by GCM wind and temperature data. This confirms that topography exerted a significant control on early Martian precipitation patterns and reinforces previous evidence [e.g., *Craddock and Howard*, 2002; *Hynek and Phillips*, 2003; *Barnhart et al*., 2009; *Hoke and Hynek*, 2009; *Luo and Stepinski*, 2009; *Som et al*., 2009; *Hynek et al*., 2010; *Mest et al*., 2010; *Irwin et al*., 2011] that the water that flowed through the valley networks originated in the atmosphere, not through melting of ground ice [*Gulick*, 2001]. Recently, *Matsubara et al*. [2013] showed that valley networks with the observed morphometry can form in a more arid climate if precipitation is orographically enhanced at high altitudes; in light of our results, this may indicate that ancient Mars was more arid than previously thought.

[23] This work has helped to constrain the CO_2 inventory of ancient Mars: since valley distribution is consistent with emplacement by orographic snowfall, our results require a late Noachian–early Hesperian atmosphere with surface pressure of at least a few hundred millibars to create a surface lapse rate, allowing preferential preservation of highland snow deposits for long intervals between melt episodes [*Wordsworth et al*., 2013], but are most consistent with surface pressure below 2 bars. Erosion rates in this scenario would have been controlled by the characteristics of the intermittent warm climate required to cause melting. Future GCM studies including the greenhouse effects of warming by impacts [e.g., *Segura et al*., 2002] or sulfur volatiles [e.g., *Halevy and Head*, 2012] will constrain plausible melting rates and the possible role of transient rainfall.

5. Conclusions

[24] Previous studies [*Burr et al*., 2009; *Luo and Stepinski*, 2009; *Grant et al*., 2011; *Irwin et al*., 2011; *Grant and Wilson*, 2012] have suggested that orographic precipitation could have been important in the early Martian climate, but ours is the first to demonstrate this quantitatively. We have shown that on an early Mars warmed only by CO_2, orographic lifting would have strongly enhanced snowfall where the densest valleys are observed, providing local-scale evidence for a precipitation origin for the valley networks. Our results at Warrego Valles, where topographic relief is sufficiently high that flow regimes differ between climates with different CO_2 surface pressures, support a late Noachian surface pressure below 2 bars. Our results build on the icy highland model [*Wordsworth et al*., 2013] by describing the effects of this climate at the scale of geological analysis.

[25] **Acknowledgments.** Thanks are extended to W. Tennant for the wind rose GrADS script and B. Hynek for valley network GIS shapefiles. We gratefully acknowledge the NASA Graduate Student Researchers Program (GSRP) grant to KES from the NASA Langley Research Center and a grant from the NASA Mars Data Analysis Program (MDAP) to JWH. We thank two anonymous reviewers for thorough and constructive reviews that improved the paper.

[26] The Editor thanks two anonymous reviewers for their assistance in evaluating this paper.

References

Ansan, V., and N. Mangold (2006), New observations of Warrego Valles, Mars: Evidence for precipitation and surface runoff, *Planet. Space Sci.*, *54*(3), 219–242.

Balme, M. R., N. Mangold, D. Baratoux, F. Costard, M. Gosselin, P. Masson, P. Pinet, and G. Neukum (2006), Orientation and distribution of recent gullies in the southern hemisphere of Mars: Observations from High Resolution Stereo Camera/Mars Express (HRSC/MEX) and Mars Orbiter Camera/Mars Global Surveyor (MOC/MGS) data, *J. Geophys. Res.*, *111*, E05001, doi:10.1029/2005JE002607.

Barnhart, C. J., A. D. Howard, and J. M. Moore (2009), Long-term precipitation and late-stage valley network formation: Landform simulations of Parana Basin, Mars, *J. Geophys. Res.*, *114*, E01003, doi:10.1029/2008JE003122.

Barstad, I., and R. B. Smith (2005), Evaluation of an orographic precipitation model, *J. Hydrometeorol.*, *6*(1), 85–99.

Burr, D. M., M. T. Enga, R. M. E. Williams, J. R. Zimbelman, A. D. Howard, and T. A. Brennand (2009), Pervasive aqueous paleoflow features in the Aeolis/Zephyria Plana region, Mars, *Icarus*, *200*(1), 52–76.

Carr, M. H. (1983), Stability of streams and lakes on Mars, *Icarus*, *56*(3), 476–495.

Costard, F., F. Forget, N. Mangold, and J. Peulvast (2002), Formation of recent Martian debris flows by melting of near-surface ground ice at high obliquity, *Science*, *295*(5552), 110–113.

Craddock, R. A., and A. D. Howard (2002), The case for rainfall on a warm, wet early Mars, *J. Geophys. Res.*, *107*(E11), 5111, doi:10.1029/2001JE001505.

Crochet, P., T. Johannesson, T. Jonsson, O. Sigurdsson, H. Bjonsson, F. Palsson, and I. Barstad (2007), Estimating the spatial distribution of precipitation in Iceland using a linear model of orographic precipitation, *J. Hydrometeorol.*, *8*(6), 1285–1306.

Dickson, J. L., J. W. Head, and M. Kreslavsky (2007), Martian gullies in the southern mid-latitudes of Mars: Evidence for climate-controlled formation of young fluvial features based upon local and global topography, *Icarus*, *188*(2), 315–323.

Fassett, C. I., and J. W. Head (2008), The timing of Martian valley network activity: Constraints from buffered crater counting, *Icarus*, *195*(1), 61–89.

Forget, F., R. M. Haberle, F. Montmessin, B. Levrard, and J. W. Head (2006), Formation of glaciers on Mars by atmospheric precipitation at high obliquity, *Science*, *311*(5759), 368–371.

Forget, F., R. Wordsworth, E. Millour, J. B. Madeleine, L. Kerber, J. Leconte, E. Marcq, and R. M. Haberle (2013), 3D modelling of the early Martian climate under a denser CO_2 atmosphere: Temperatures and CO_2 ice clouds, *Icarus*, *222*(1), 81–99.

Gaidos, E., and G. Marion (2003), Geological and geochemical legacy of a cold early Mars, *J. Geophys. Res.*, *108*(E6), 5055, doi:10.1029/2002JE002000.

Giambelluca, T. W., M. A. Nullet, T. A. Schroeder (1986), Rainfall atlas of Hawai'i, *Report R76*, State of Hawai'i Department of Land and Natural Resources, Division of Water and Land Development, Honolulu, HI.

Grant, J. A., and S. A. Wilson (2012), A possible synoptic source of water for alluvial fan formation in southern Margaritifer Terra, Mars, *Plan. Space Sci.*, *72*(1), 44–52.

Grant, J. A., R. P. Irwin, S. A. Wilson, D. Buczkowski, and K. Siebach (2011), A lake in Uzboi Vallis and implications for Late Noachian–Early Hesperian climate on Mars, *Icarus*, *212*(1), 110–122.

Gulick, V. C. (2001), Origin of the valley networks on Mars: a hydrological perspective, *Geomorphologie*, *37*(3–4), 241–268.

Halevy, I., and J. W. Head (2012), Punctuated volcanism, transient warming and global change in the late Noachian-early Hesperian, paper presented at the 43rd Lunar and Planetary Science Conference, Lunar and Planetary Institute, The Woodlands, TX.

Hoke, M. R. T., and B. M. Hynek (2009), Roaming zones of precipitation on ancient Mars as recorded in valley networks, *J. Geophys. Res.*, *114*, E08002, doi:10.1029/2008JE003247.

Houze, R. A. (2012), Orographic effects on precipitating clouds, *Rev. Geophys.*, *50*, RG1001, doi:10.1029/2011RG000365.

Hughes, M., A. Hall, and R. G. Fovell (2009), Blocking in areas of complex topography, and its influence on rainfall distribution, *J. Atmos. Sci.*, *66*(2), 508–518.

Hynek, B. M., and R. J. Phillips (2003), New data reveal mature, integrated drainage systems on Mars indicative of past precipitation, *Geology*, *31*(9), 757–760.

Hynek, B. M., M. Beach, and M. R. T. Hoke (2010), Updated global map of Martian valley networks and implications for climate and hydrologic processes, *J. Geophys. Res.*, *115*, E09008, doi:10.1029/2009JE003548.

Irwin, R. P., and A. D. Howard (2002), Drainage basin evolution in Noachian Terra Cimmeria, Mars, *J. Geophys. Res.*, *107*(E7), 5056, doi:10.1029/2001JE001818.

Irwin, R. P., R. A. Craddock, A. D. Howard, and H. L. Flemming (2011), Topographic influences on development of Martian valley networks, *J. Geophys. Res.*, *116*, E02005, doi:10.1029/2010JE003620.

Kerber, L. K., F. Forget, J.-B. Madeleine, R. Wordsworth, J. W. Head, and L. Wilson (2013), The effect of atmospheric pressure on the dispersal of pyroclasts from Martian volcanoes, *Icarus*, *223*(1), 149–156.

Kreslavsky, M. A., J. W. Head, and D. R. Marchant (2008), Periods of active permafrost layer formation during the geological history of Mars: Implications for circum-polar and mid-latitude surface processes, *Planet. Space Sci.*, *56*(2), 289–302.

Luo, W., and T. F. Stepinski (2009), Computer-generated global map of valley networks on Mars, *J. Geophys. Res.*, *114*, E11010, doi:10.1029/2009JE003357.

Matsubara, Y., A. D. Howard, and S. A. Drummond (2011), Hydrology of early Mars: Lake basins, *J. Geophys. Res.*, *116*, E04001, doi:10.1029/2010JE003739.

Matsubara, Y., A. D. Howard, and J. P. Gochenour (2013), Hydrology of early Mars: Valley network incision, *J. Geophys. Res. Planets*, *118*, 1365–1387, doi:10.1002/jgre.20081.

Mest, S. C., D. A. Crown, and W. Harbert (2010), Watershed modeling in the Tyrrhena Terra region of Mars, *J. Geophys. Res.*, *115*, E09001, doi:10.1029/2009JE003429.

Minder, J. R., D. R. Durran, G. H. Roe, and A. M. Anders (2008), The climatology of small-scale orographic precipitation over the Olympic Mountains: Patterns and processes, *Q. J. Roy. Meteor. Soc.*, *134*(633), 817–839.

Montmessin, F., P. Rannou, and M. Cabane (2002), New insights into Martian dust distribution and water-ice cloud microphysics, *J. Geophys. Res.*, *107*(E6), 5037, doi:10.1029/2001JE001520.

Morgan, G. A., J. W. Head, F. Forget, J. B. Madeleine, and A. Spiga (2010), Gully formation on Mars: Two recent phases of formation suggested by links between morphology, slope orientation and insolation history, *Icarus*, *208*(2), 658–666.

Roe, G. H. (2005), Orographic precipitation, *Annu. Rev. Earth. Pl. Sc.*, *33*, 645–671.

Segura, T. L., O. B. Toon, A. Colaprete, and K. Zahnle (2002), Environmental effects of large impacts on Mars, *Science*, *298*(5600), 1977–1980.

Smith, R. B. (2006), Progress on the theory of orographic precipitation, *GSA Spec. Pap.*, *398*, 1–16.

Smith, R. B., and I. Barstad (2004), A linear theory of orographic precipitation, *J. Atmos. Sci.*, *61*(12), 1377–1391.

Smith, R. B., I. Barstad, and L. Bonneau (2005), Orographic precipitation and Oregon's climate transition, *J. Atmos. Sci.*, *62*(1), 177–191.

Som, S. M., D. R. Montgomery, and H. M. Greenberg (2009), Scaling relations for large Martian valleys, *J. Geophys. Res.*, *114*, E02005, doi:10.1029/2008JE003132.

Squyres, S. W., and J. F. Kasting (1994), Early Mars: How warm and how wet?, *Science*, *265*(5173), 744–749.

Wallace, D., and C. Sagan (1979), Evaporation of ice in planetary atmospheres: Ice-covered rivers on Mars, *Icarus*, *39*(3), 385–400.

Williams, K. E., O. B. Toon, J. L. Heldmann, and M. T. Mellon (2009), Ancient melting of mid-latitude snowpacks on Mars as a water source for gullies, *Icarus*, *200*(2), 418–425.

Wordsworth, R. D., F. Forget, F. Selsis, E. Millour, B. Charnay, and J. B. Madeleine (2011), Gliese 581d is the first discovered terrestrial-mass exoplanet in the habitable zone, *Astrophys. J. Lett.*, *733*(2).

Wordsworth, R. D., F. Forget, E. Millour, J. W. Head, J. B. Madeleine, and B. Charnay (2013), Global modelling of the early Martian climate under a denser CO_2 atmosphere: Water cycle and ice evolution, *Icarus*, *222*(1), 1–19.